Chemistry and Physics of Lipids 220 (2019) 36–48

Contents lists available at ScienceDirect

Chemistry and Physics of Lipids

journal homepage: www.elsevier.com/locate/chemphyslip

Lipidomic analysis of meibomian gland secretions from the tree shrew: Identification of candidate tear lipids critical for reducing evaporation

Jianzhong Chen*, Shyam Panthi[1]

Department of Optometry and Vision Science, University of Alabama at Birmingham, Birmingham, AL, 35294, USA

ARTICLE INFO

Keywords:
Electrospray ionization
Tandem mass spectrometry
MSMS^{all}
Meibomian gland secretion
Wax esters
Cholesteryl esters
Diesters
Phospholipids
Sphingolipids
(*O*-acyl)-ω-hydroxy fatty acids
Tree shrew
Dry eye
Evaporative

ABSTRACT

Lipids secreted from the meibomian glands form the outermost layer of the tear film and reduce its evaporation. Abnormal changes in the quantities or compositions of lipids present in meibomian gland secretions (meibum) are known to lead to dry eye disease, although the underlying mechanism is not yet well understood. The tree shrew is the non-primate mammal most closely related to humans. To assess the utility of the tree shrew as a model for the study of dry eye disease, we analyzed the lipid profile of tree shrew meibum using an untargeted ESI-MS and MS/MS^{all} shotgun approach. The resulting lipidome shared many similarities with human meibum, while displaying some interesting differences. For example, several classes of lipids, including wax esters, cholesteryl esters, diesters, and (*O*-acyl)-ω-hydroxy fatty acids, had relatively longer chain lengths in tree shrew meibum. These increases in length may promote more effective reduction of tear evaporation in the tree shrew, which likely underlies the much longer blinking interval of this mammal. Our results suggest that the tree shrew could be an effective model for the study of dry eye.

1. Introduction

Lipids secreted from the meibomian glands, located posterior to the eyelashes on the eyelid margin, form the outermost layer of tear film (Willcox et al., 2017). This lipid layer, which has a mean thickness of 42 nm (King-Smith et al., 2010), overlays the mucous and aqueous layers (collectively referred to as the mucoaqueous layer) to form a tear film approximately 3 μm thick (Willcox et al., 2017). The tear film covers the surface of the cornea and keeps it lubricated to support normal eye function (Willcox et al., 2017). An abnormal lipid layer is believed to promote rapid tear evaporation and can eventually lead to the development of evaporative dry eye disease (DED) (Chen et al., 2017; Foulks, 2007). Meibomian gland dysfunction (MGD) is the most common reason for abnormal lipid secretion, which produces an abnormal lipid layer (Tomlinson et al., 2011). However, it is currently difficult to detect abnormal lipid secretion at an early, asymptomatic stage, and the mechanisms underlying reduction of evaporation in the context of a normal lipid layer are still not well understood. An improved understanding of the overall lipid composition of healthy meibum at the molecular level will help with the detection of MGD and DED at an early stage, in addition to facilitating the development of strategies for early intervention.

The lipid composition of human meibum has been studied extensively using mass spectrometry, beginning with characterization of the lipid moieties after hydrolysis and derivatization (Mathers and Lane, 1998; Nicolaides et al., 1981). Spectroscopic methods have also been used to characterize the functional groups present in meibum lipids (Borchman et al., 2012, 2015; Shrestha et al., 2011). Advances in mass spectrometry, including development of the soft ionization methods of atmospheric pressure chemical ionization (APCI) and electrospray ionization (ESI), have facilitated characterization of meibum lipids at the molecular level over the last decade or so (Butovich et al.,

Abbreviations: APCI, atmospheric pressure chemical ionization; CE, cholesteryl ester; DE, diester; DED, dry eye disease; DE-I, ω Type I-St diester; DE-II, α,ω Type II diester; ESI, electrospray ionization; FA, fatty acid; FAl, fatty alcohol; FFA, free fatty acid; HPLC, high-performance liquid chromatography; LPC, lysophosphatidylcholine; LPE, lysophosphatidylethanolamine; LPI, lysophosphatidylinositol; MGD, meibomian gland dysfunction; MS, mass spectrometry; MS/MS, tandem mass spectrometry; Neg, negative; OAHFA, (*O*-acyl)-ω-hydroxy fatty acid; PC, phosphatidylcholine; PE, phosphatidylethanolamine; PI, phosphatidylinositol; PIS, precursor ion scanning; pNLS, pseudo neutral loss scanning; Pos, positive; pPIS, pseudo precursor ion scanning; PS, phosphatidylserine; SM, sphingomyelin; TG, triacylglycerol; TIC, total ion chromatogram; TOF, time-of-flight; WE, wax ester

* Corresponding author.
E-mail address: jzchen@uab.edu (J. Chen).
[1] Current address: Department of Ophthalmology, University of Tennessee Health Science Center, Memphis, TN, 38103, USA.

https://doi.org/10.1016/j.chemphyslip.2019.01.003
Received 4 December 2018; Received in revised form 8 January 2019; Accepted 14 January 2019
Available online 17 January 2019
0009-3084/

2007; Chen et al., 2010). The major lipid components of human meibum that have been reported are wax esters (WEs); cholesteryl esters (CEs); diesters (DEs), including ω Type I-St diesters (DE-Is) and α,ω Type II diesters (DE-IIs); triacylglycerols (TGs); free fatty acids (FFAs); and (*O*-acyl)-ω-hydroxy fatty acids (OAHFAs) (Brown et al., 2013; Butovich et al., 2007; Chen et al., 2010; Lam et al., 2011; Mathers and Lane, 1998; Nicolaides et al., 1981; Nicolaides and Santos, 1985).

Recently, we have modified the shotgun lipidomics approach (Chen et al., 2010; Han and Gross, 2005; Han et al., 2012) by including MS/MS^{all} (Simons et al., 2012) and sequential switching between two polarity modes. This improved approach was successfully applied to perform comprehensive, untargeted analysis of human meibum using quantities as low as 8 µL (Chen and Nichols, 2018). More than 600 molecular species were detected with a high signal-to-noise ratio (S/N) (Chen and Nichols, 2018). With this new approach, MS/MS of all precursor ions in the *m/z* range of interest were acquired in both positive and negative ion modes. Similar to targeted analyses, such as precursor ion scanning (PIS), this untargeted analysis, termed pseudo precursor ion scanning (pPIS), had a higher sensitivity for low-abundance lipids, such as phospholipids (Chen and Nichols, 2018; Saville et al., 2011). Furthermore, this approach yields full MS/MS spectra for in-depth analyses.

Animal models, such as rats and mice, are often used to study MGD and DED (Barabino et al., 2004; Barabino and Dana, 2004). One limitation of these models is that these animals are not close to humans, thus their pathology may not closely resemble that of humans. In contrast, tree shrews (*Tupaia glis belangeri*), small mammals closely related to primates that can be maintained at a much lower cost (Cao et al., 2003), have previously been employed in investigation of myopia (Norton, 1999) and could be an ideal model for MGD and DED studies. However, there is little information in the literature about on the meibomian glands of the tree shrew (Lukoschus et al., 1984; Montagna et al., 1962), and the lipid composition of tree shrew meibum has never been reported. A comparison of the lipid profiles of tree shrew and human meibum will, therefore, help to evaluate the validity of tree shrew as an animal model for DED. Moreover, the tree shrew has much lower blinking frequency than humans (< 1 per minute vs. 14 per minute) (Stevens and Livermore, 1978), which implies a higher tear film stability (Inomata et al., 2018). As a result, differences in the lipid profiles could identify candidate lipids important for reducing tear evaporation.

In the present study, we applied the MS/MS^{all} approach to characterize the lipid composition of tree shrew meibum. This lipid profile was then compared to our recent report of the composition of human meibum (Chen and Nichols, 2018), along with other related studies, to identify similarities and differences.

2. Materials and methods

2.1. Chemicals

Chloroform (HPLC grade, > 99.9%, with amylene as the stabilizer), methanol (LC–MS grade, > 99.9%), and ammonium hydroxide solution (25%, eluent additive for LC–MS, Fluka) were purchased from Sigma-Aldrich (St. Louis, MO, USA).

2.2. Tree shrew meibum sample collection

Eyelids were removed from two sacrificed 10-week-old female tree shrews (UAB tree shrew core facility, Birmingham, AL) used for unrelated studies. These other studies had no effect on meibum composition. For each eyelid, a sterile spatula was placed towards the inner conjunctival side of the eyelid (Fig. 1), and the meibum was expressed from the meibomian glands by pressing on the eyelid from the outer skin side using a finger. Images of meibum expression were captured using a Zeiss Axioplan 2 microscope (Carl Zeiss Meditec, Inc.; Dublin, CA, USA) under bright field illumination at 10× magnification. Samples were collected from the orifice of the meibomian gland in the eyelid margin using 32-mm, 0.5-µL glass microcapillary tubes (Drummond; Broomall, PA, USA) in a tapping motion. This procedure was similar to that described in previous reports (Chen et al., 2013), although the quantity of meibum collected from tree shrew eyelids was less than that typically collected from humans. The microcapillary tubes were placed in a glass vial and stored immediately at -20 °C until further extraction and mass spectrometric evaluation.

2.3. Mass spectrometry analysis

The procedures for sample preparation were similar to that described in previous reports (Chen et al., 2010, 2013; Chen and Nichols, 2018). Briefly, each meibum sample was directly dissolved in 100 µL of a chloroform-methanol solvent mixture (2:1, vol/vol) in a glass sample vial. Due to the small quantities of tree shrew meibum samples, the lipids collected in the microcapillary glass tubes were barely visible. Unlike the previous procedure for human meibum samples, a bulb was used to rinse the capillary with the solvent mixture by aspirating and dispensing several times to maximize lipid recovery. No multi-phase separation was performed because meibum is almost exclusively composed of neutral lipids with negligible amounts of other species (Linton et al., 1961). The resulting solution was then diluted five-fold with methanol, and 0.025% ammonium hydroxide was included as the additive. No plastics were used during sample preparation, with the exception of Teflon in the syringes.

The procedures for mass spectrometry data acquisition were similar to those described in a previous report (Chen and Nichols, 2018). Briefly, the diluted working solution was directly infused into an ESI quadrupole time-of-flight (TOF) mass spectrometer (TripleTOF 5600; SCIEX; Concord, Canada) with a built-in syringe pump. MS and MS/MS^{all} data was acquired. The same solution was successively analyzed in both modes. In positive ion mode, a voltage of 5500 V and a de-clustering potential of 40 V were applied, with a collision energy of 10 eV for MS, or a collision energy of 40 eV with a collision energy spread of 40 eV for MS/MS^{all}. In negative ion mode, a voltage of 4500 V and a de-clustering potential of -40 V were applied, with a collision energy of 20 eV for MS, or a collision energy of −54 eV with a collision energy spread of 40 eV for MS/MS^{all}. The flow rate was 7 µL/min, and the temperature was 250 °C. The MS signal was typically acquired for 3 min prior to MS/MS^{all} acquisition. For the MS/MS^{all} acquisition, the accumulation time for each scan was 1.5 s, which was 5 times the default acquisition time (300 ms) used in our recent report (Chen and Nichols, 2018), resulting in a total of 26 min' of acquisition in each mode. A total of 1000 MS/MS spectra, covering all precursor ions in the *m/z* 200–1200 range at approximately every 1-Da step, were acquired in each mode, yielding a total of 2000 MS/MS spectra for both ion modes. A list of manufacturer's pre-defined *m/z* values (Chen and Nichols, 2018), including an appropriate mass defect (Sleno, 2012), was used to define the precursor ions for MS/MS^{all} acquisition.

2.4. Data analysis

The procedures for data analysis were similar to those described in our recent report (Chen and Nichols, 2018). Briefly, the spectra were processed using PeakView software (SCIEX; Concord, Canada). Lipid species detected in MS spectra were identified manually by matching the *m/z* values (typically within 5 ppm) to a reference list of meibum lipid species. The reference lipid list was created in-house based on our previous MS and MS/MS spectra (Chen and Nichols, 2018). If the *m/z* values were not on the list, the lipids were identified by matching the *m/z* of related species of the same lipid classes with different saturation levels and chain lengths. To identify common lipid species, such as CEs, sphingomyelins (SMs), and phosphatidylcholines (PCs), we used the peak list to query Lipidmaps (http://lipidmaps.org/tools/ms/lm_mass_

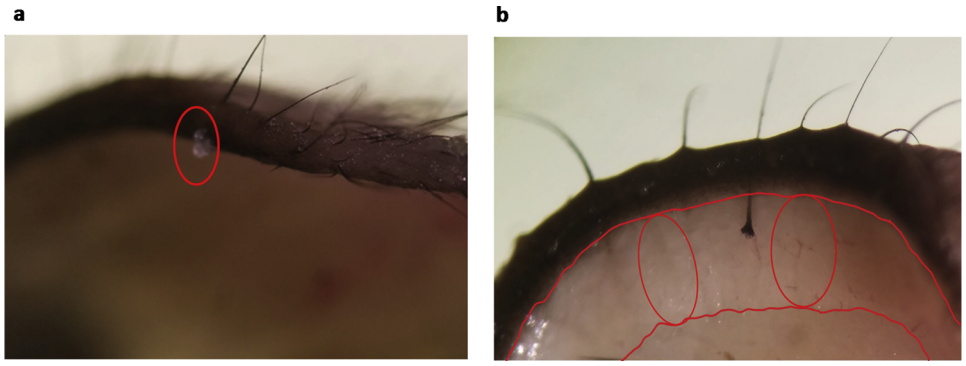

Fig. 1. Expression of meibum from meibomian glands in tree shrew eyelids. a) Meibum oozing out of a meibomian gland orifice with pressure; b) inner side of a tree shrew eyelid. The eyelid area outlined in red contains the meibomian glands, and red ovals indicate the locations of individual meibomian glands.

form.php), typically using a limit of 0.005 Da. Assignments were verified with information from the corresponding tandem mass spectra when possible. For MS/MS^{all} acquisition, we assigned peaks from pPIS spectra with the aid of the reference list mentioned above. When in doubt, we analyzed the corresponding full MS/MS spectra extracted from MS/MS^{all} acquisition to check the characteristic product ions or fragmentation patterns.

3. Results & discussion

3.1. Overview of MS and MS/MS^{all}

Tree shrew meibum was analyzed by MS and MS/MS^{all} with sequential polarity switching between negative and positive ion modes. As expected, the abundant peaks in the positive ion mode MS spectrum of tree shrew meibum corresponded to WEs, CEs, DEs, and TGs (Fig. 2, Table 1, Supplementary Table S1), while in negative ion mode, the peaks corresponded to FFAs, OAHFAs and cholesteryl sulfate (Fig. 3, Table 1, Supplementary Table S2). The presence of these abundant lipids is consistent with literature reports on human meibum lipids (Brown et al., 2013; Butovich et al., 2007, 2009; Chen et al., 2010; Chen and Nichols, 2018; Lam et al., 2014, 2011; Mathers and Lane, 1998; Mori et al., 2014; Nicolaides et al., 1981). In addition to these commonly reported lipids, some phospholipids were also detected at relatively high intensities, including PCs, phosphatidylethanolamines (PEs), phosphatidylinositols (PIs), and phosphatidylserines (PSs) (Figs. 2 & 3, Supplementary Fig. S1). However, the peak patterns of these phospholipids were different from those previously reported for human meibum (Chen and Nichols, 2018; Saville et al., 2011). It is possible that these phospholipids may have come from immature meibomian gland cells or tissues surrounding the meibomian glands, as discussed in Section 3.2.9.

MS alone is often insufficient for lipid identification. The lipids detected in MS analysis can be verified by pPIS spectra or full MS/MS spectra, extracted from MS/MS^{all} acquisition (Chen and Nichols, 2018). The pPIS method is similar to the more commonly used PIS method for the analysis of a class of lipids that yield a common product ion. PIS is typically performed on a relatively low resolution triple-quadrupole mass spectrometer (Carr et al., 1993; Huddleston et al., 1993), but has also been available on a high resolution quadrupole time-of-flight mass spectrometer since 2002 (Ekroos et al., 2002). However, one important feature of MS/MS^{all} that differs from PIS is that MS/MS^{all} acquires the full MS/MS spectrum, instead of only monitoring a few product ions (Chen and Nichols, 2018; Simons et al., 2012). As a result, in-depth

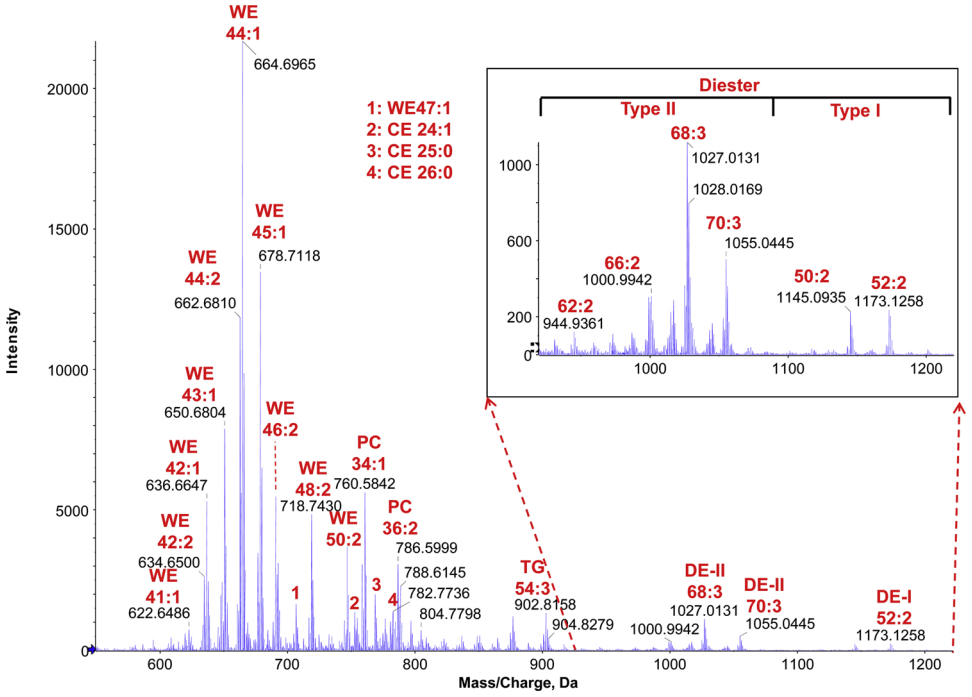

Fig. 2. Positive ion mode MS analysis of tree shrew meibum. The inset shows the *m/z* 930–1240 region, where the diester peaks are located.

Table 1
The number of molecular species for each lipid class detected in tree shrew meibomian gland secretions using different analyses.[a].

	Lipid Class		Number of Species Detected			
			MS	MS/MS^{all}		
				Pseudo precursor ion scanning [b]		Full MS/MS
Positive ion	Cholesteryl ester		30	369.352	**73**	–
	ω Type I-St diester		10		**12**	–
	Wax ester	FA16:0-	–	257.248	20	–
		FA17:0-	–	271.263	26	–
		FA18:0-	–	285.279	14	–
		FA16:1-	–	255.232	15	–
		FA17:1-	–	269.248	8	–
		FA18:1-	–	283.263	19	–
		FA18:2-	–	263.237[c]	15	–
		All	77	Sum	**117**	108
	Triacylglycerol	FA18:1-	–	265.253	25	–
		All	**40**	–	–	–
	α,ω Type II diester	FA18:1-	–	265.253[d]	12	–
		All	**23**	–	–	–
	Total		180	–	239	108
Negative ion	(*O*-acyl)-ω-hydroxy Fatty acid	FA18:1-	–	281.249	12	–
		FA24:1-	–	365.342	9	–
		All	34	–	–	**106**
	Free fatty acid		**58**	–	–	–
	Cholesteryl sulfate		1	–	–	**1**
	Sum		93	–	21	107
	Total		273	–	260	215
Grand Total			430[e]			

[a] Phospholipids were also detected, but likely originated from immature cells or contamination from surrounding tissues, rather than meibum. For more detail, see Table 2.

[b] The tolerance range for the precursor ions was ± 0.025.

[c] Unlike the other wax esters whose protonated-fatty-acid product ions were used for their detection from pseudo precursor ion scanning (pPIS), FA18:2-based wax esters were detected from pPIS by using their protonated-fatty acid 18:2 along with the loss of a water molecule (FA 18:2 – H_2O) as the product ion due to its higher intensity.

[d] Pseudo neutral loss scanning was also performed.

[e] The grand total number of species was calculated by adding the total number of species highlighted in bold text.

information about the lipid composition of each class can be obtained from pPIS spectra or full MS/MS spectra. This in-depth information includes data showing the presence of lipid isomers, i.e., lipids of the same molecular weight, but different structures. If needed, this stored information can be analyzed in the future as new species are identified.

By analyzing representative MS/MS spectra of the major classes of lipids present in meibum (Figs. 4 & 5), the characteristic product ions or neutral losses can be used to extract information for these classes of lipids. Some lipid classes share a common, characteristic product ion. For example, CEs and DE-Is generate a common product ion, *m/z* 369.3516 (Figs. 4c, 5 b & d), while PCs and SMs generate a different common product ion, *m/z* 184.0733 (Fig. 4b). Precursors of these common product ions (Figs. 6 & 7) can be extracted from MS/MS^{all} total ion chromatograms (TICs) to generate pPIS spectra (Chen and Nichols, 2018). In contrast, some other classes of lipids only generate FA moiety-based characteristic product ions that depend on the FA moiety therein. For example, WEs generate product ions *m/z* 285.2788, *m/z* 283.2632, and *m/z* 281.2475 for FA 18:0, FA 18:1, and FA 18:2 moiety-containing WEs, respectively, along with additional ions corresponding to loss of one or two water molecules for the latter unsaturated FA moieties (Fig. 4a). Therefore, for these classes of lipids, a series of pPIS spectra are needed to obtain a complete view of the lipids (Chen and Nichols, 2018). To use pPIS to detect the lipids with high sensitivity, while minimizing interference from unrelated species, a tolerance of ± 0.025 *m/z* from the product ion was found to be optimal under the experimental conditions used for this study. Major lipids detected by MS/MS^{all} are discussed in the following sections.

3.2. Lipid classes detected

3.2.1. Cholesteryl esters

From MS analysis, a total of 30 CEs were detected (Fig. 2, Supplementary Table 1, Supplementary Fig. 1). The S/N was not high for some of these peaks due to overlap. In contrast, in the pPIS spectrum of *m/z* 369.352 ± 0.025 (the common product ion of CEs), high S/N CE peaks ranging from 16:1 to 36:1 were detected (Figs. 4c & 6, Supplementary Table S3, and Supplementary Figs. S2–S7). The most abundant CEs in both MS and MS/MS^{all} were 24:0. 25:0, 26:0, and 27:0 (Fig. 6, Supplementary Fig. 1), consistent with previously reported CEs in human meibum (Chen et al., 2013; Chen and Nichols, 2018). Note that unsaturated CEs typically showed a higher response than their saturated counterparts under the same experimental conditions (Chen et al., 2013), and the responses of monounsaturated CEs were approximately double that of their saturated counterparts under the experimental conditions analyzed (Chen and Nichols, 2018).

In addition to these predominantly saturated CEs, there appears to be another subgroup of monounsaturated CEs with much longer carbon chains. In the pPIS spectrum, these peaks centered around CE 32:1 and included CE 28:1, 30:1, 32:1, 34:1, and 36:1 (Fig. 6). In the MS spectrum (Supplementary Fig. S1), the center of the series of peaks appeared to shift downward to CE 30:1; however, a closer look at the peaks revealed that CE 30:1 partially overlapped with TG 49:1, which increased the intensity of CE 30:1 peak. Therefore, the relative peak intensity values were more reliable in the pPIS spectrum. The overall chain length of this subgroup of CEs in tree shrew meibum, as displayed in Fig. 6, is longer than that in human meibum, which centered on 30:1 (Brown et al., 2013; Chen and Nichols, 2018; Lam et al., 2011).

3.2.2. ω Type I-St diesters

DE-I is one of two major classes of DEs present in human meibum (Butovich et al., 2011, 2012; Chen et al., 2010; Nicolaides and Santos, 1985). A total of 10 and 12 DE-I molecular species were detected in the MS (Fig. 1, Supplementary Table S1) and pPIS (Fig. 7, Supplementary Table S3) spectra, respectively. The compositions of the lipid species of this class present in tree shrew (Fig. 7, Supplementary Table 3, and Supplementary Figs. S7 & S8) are quite similar to those in human meibum (Chen et al., 2010; Chen and Nichols, 2018). However, as observed for CEs, the overall chain length of DE-Is was longer in tree shrew meibum compared to human meibum. In the MS spectrum, the compositions of the most abundant DE-I species in tree shrew were 50:2 and 52:2, at about the same intensity (Fig. 1). In the pPIS spectrum, the most abundant DE-I is 52:2 (Fig. 7), which is longer than the most abundant DE-I in human meibum, i.e., 50:2 (Chen and Nichols, 2018).

3.2.3. Wax esters

In the MS spectrum, a total of 77 WEs were detected. The overall chain length of WEs in tree shrew centered around WE 44:1 (Fig. 1, Supplementary Table S1). In contrast, in human meibum, WE 42:1 and 44:1 were about the same intensity, and the center appeared to be WE 43:1 (Chen and Nichols, 2018). Whether the shift is in the FA or FAl moiety of the WE cannot be determined from the MS spectrum. However, they can be determined from the pPIS spectrum as discussed below (Figs. 8–10, and Supplementary Figs. S10-S17).

Unlike CEs and DE-Is that share a common product ion, detection of WEs from pPIS spectra is more complicated. A series of characteristic product ions is generated based on the fatty acid moiety of the WE (Chen et al., 2015, 2016). As a result, a series of pPIS spectra were required to fully analyze WEs. Based on the pPIS spectra, the compositions of the WE lipid species in tree shrew meibum (Figs. 8–10, Supplementary Figs. S10–S17, and Supplementary Table S3) is quite similar

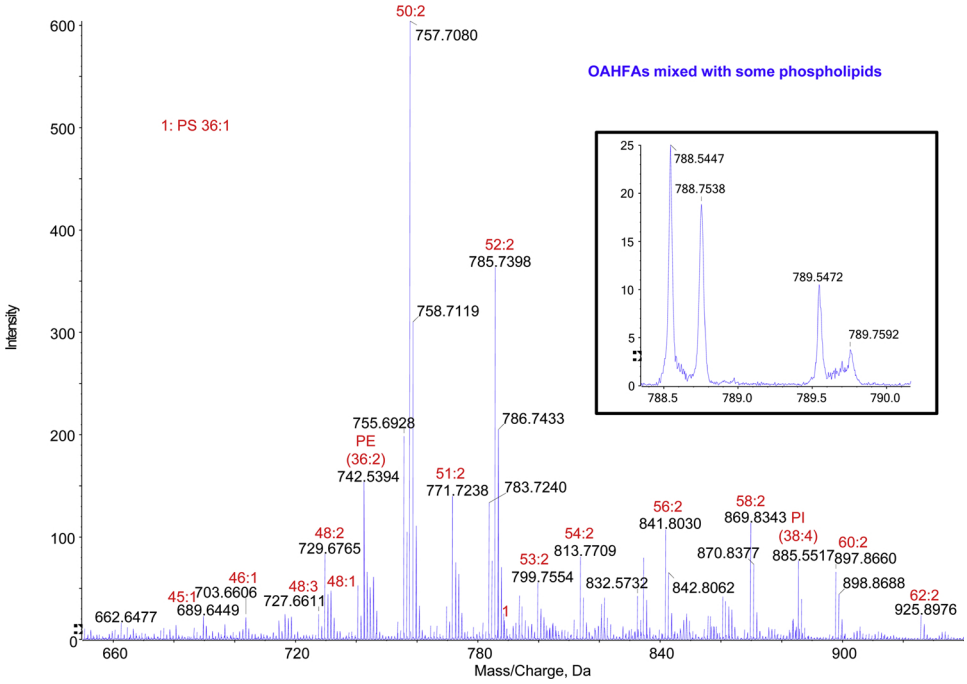

Fig. 3. Negative ion mode MS analysis of tree shrew meibum. Only the m/z 650–940 region is shown. Most of the peaks correspond to (*O*-acyl)-ω-hydroxy fatty acids (OAHFAs). For clarity, OAHFA label was omitted, but peaks corresponding to phospholipids, including phosphatidylethanolamine (PE), phosphatidylserine (PS), and phosphatidylinositol (PI) are labeled. The two numbers labeling each peak, separated by a colon, represent the total number of carbon atoms and the number of double bonds for OAHFAs, and the total number of carbon atoms and the number of double bonds for fatty acyl chains of the phospholipids.

to those in human meibum (Chen et al., 2010; Chen and Nichols, 2018). The most abundant FAl present in WEs is FAl 26:0 for both tree shrew meibum (Figs. 8–10, Supplementary Figs. S13-S17) and human meibum (Brown et al., 2013; Chen et al., 2016; Chen and Nichols, 2018). However, compared to human meibum, the overall chain length of the FAl moieties in WEs in tree shrew meibum was also longer. In the tree shrew, FAl 27:0 is the second most abundant FAl moiety and has a peak intensity much higher than the other FAl moieties, except for FAl 26:0 (Figs. 8–10, Supplementary Figs. S13-S17). In contrast, in humans, FAl 25:0 and FAl 24:0 are two next most abundant FAl moieties, while FAl 27:0 is much less abundant (Brown et al., 2013; Chen et al., 2016; Chen and Nichols, 2018).

The total number of WEs detected by MS/MS^{all} can be calculated in two ways. One is by summing up the number of WEs identified from each pPIS spectra, which yields a result of 117 WEs. The other method is manual analysis (Chen et al., 2015, 2016; Chen and Nichols, 2018) of each MS/MS spectrum from the MS/MS^{all} acquisition, which yields a total of 108 species (Supplementary Table. S5). In contrast, a total of

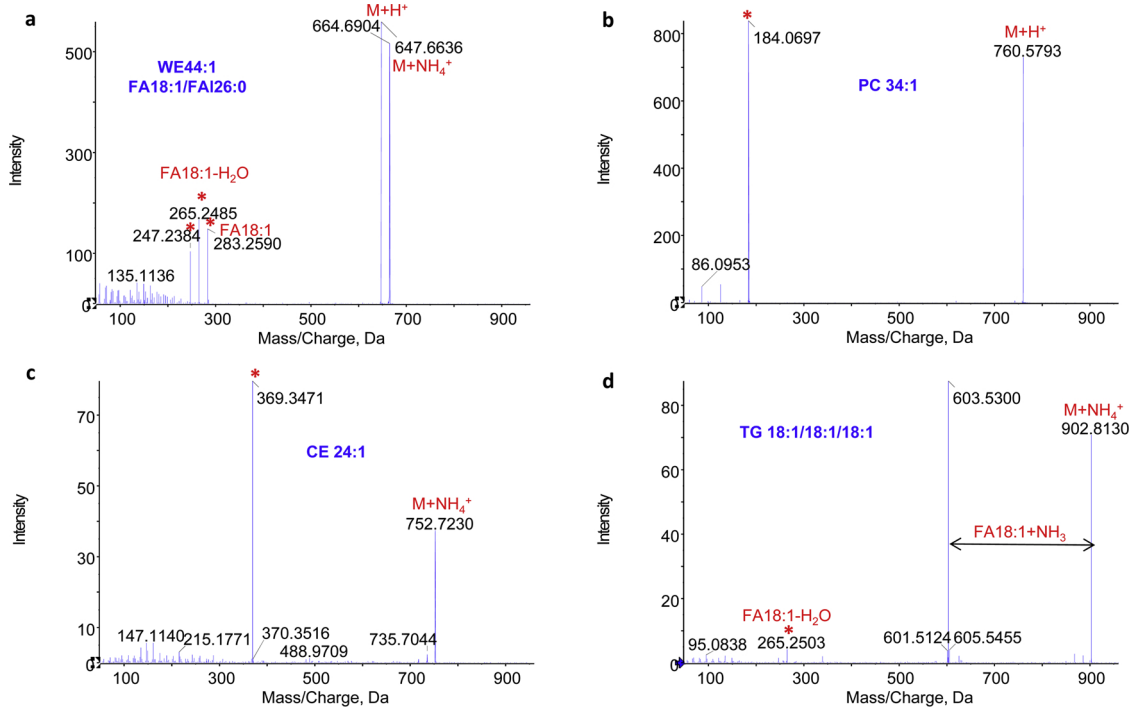

Fig. 4. Representative MS/MS spectra extracted from positive ion mode MS/MS^{all} acquisition of tree shrew meibum. a) Wax ester (WE) 44:1; b) phosphatidylcholine (PC) 34:1; c) cholesteryl ester (CE) 24:1; d) triacylglycerol (TG) 54:3. The characteristic product ions are labeled with asterisks (*). The combinations of the moieties for the major molecular species are shown. Ions corresponding to ammoniated and protonated lipids are labeled M + NH_4^+ and M + H^+, respectively. Abbreviations for the product ions are as follows: FA, protonated fatty acid; FAl, fatty alcohol.

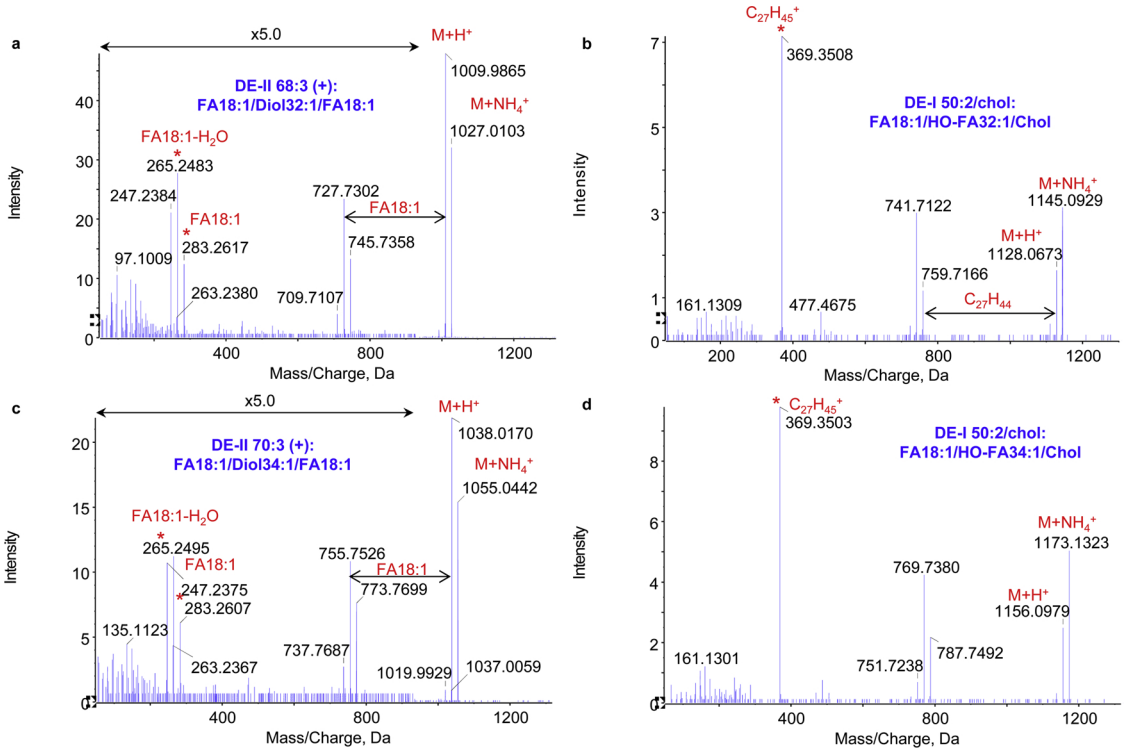

Fig. 5. Representative MS/MS spectra extracted from positive ion mode MS/MS^{all} acquisition of tree shrew meibum. a) α, ω Type II diester (DE-II) 68:3; b) ω Type I-St diester (DE-I) 50:2; c) α, ω Type II diester (DE-II) 70:3; and d) ω Type I-St diester (DE-I) 52:2. The characteristic product ions are labeled with asterisks (*). The combinations of the moieties for the major molecular species are shown. Ions corresponding to ammoniated and protonated lipids are labeled M + NH_4^+ and M + H^+, respectively. Abbreviations for the product ions and lipid moieties are as follows: FA, fatty acid; FAl, fatty alcohol; HO-FA, hydroxy fatty acid; Chol, cholesteryl.

130 and 163 WEs were found to be present in human meibum (Chen and Nichols, 2018). These higher values are likely due to the higher S/N for human meibum samples.

3.2.4. α,ω Type II diesters

In the MS spectrum, a total of 23 DE-IIs were detected (Supplementary Table S1). The compositions of the DE-II lipid species in tree shrew meibum (Figs. 2) appeared similar to those present in human meibum (Chen and Nichols, 2018). However, compared to human meibum, the overall chain length of Type-II DEs in tree shrew meibum was longer (Fig. 2). Although the most abundant DE-II in tree shrew meibum (Fig. 2) was the same as in human meibum (Chen et al., 2010, 2013; Chen and Nichols, 2018), i.e. 68:3, the second most abundant DE-II in tree shrew meibum was of much longer chain than in

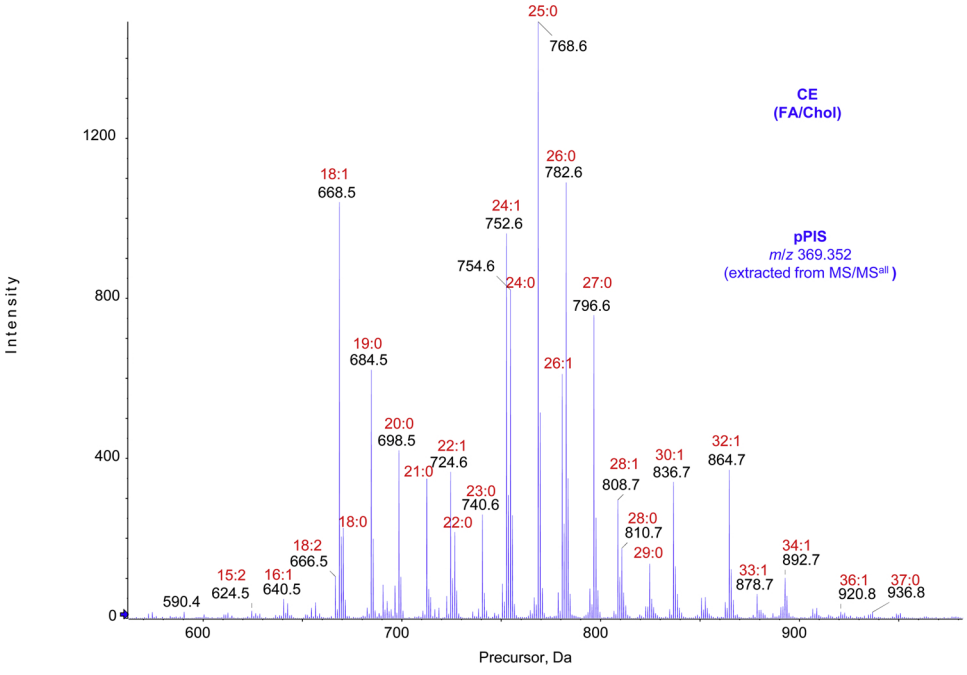

Fig. 6. Pseudo precursor ion scanning (pPIS) spectrum of *m/z* 369.352 ± 0.025 extracted from positive ion mode MS/MS^{all} analysis of tree shrew meibum. Only the cholesteryl ester (CE) region is shown. Abbreviations for the lipid moieties are as follows: FA, fatty acid; Chol, cholesteryl. The two numbers labeling each peak, separated by a colon, represent the total number of carbon atoms in the lipid ion, excluding the cholesteryl moiety, and the number of double bonds.

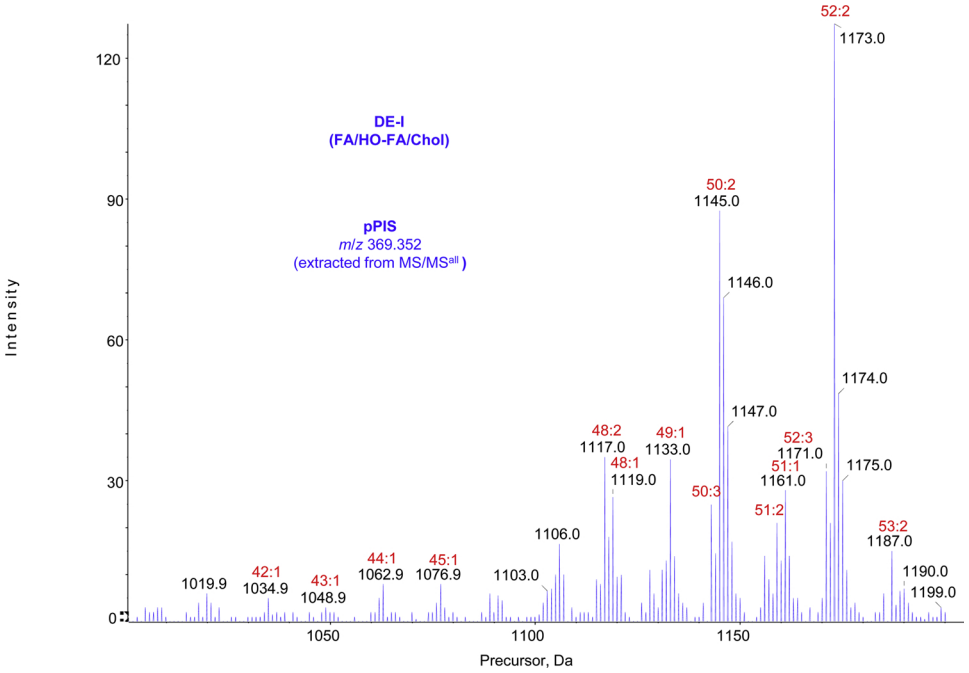

Fig. 7. Pseudo precursor ion scanning (pPIS) spectrum of *m/z* 369.352 ± 0.025 extracted from positive ion mode MS/MS^{all} analysis of tree shrew meibum. Only the ω Type I-St diester (DE-I) region is shown. Abbreviations for the lipid moieties are as follows: FA, fatty acid; HO-FA, hydroxy fatty acid; Chol, cholesteryl. The two numbers labeling each peak, separated by a colon, represent the total number of carbon atoms in the lipid ion, excluding the cholesteryl moiety, and the number of double bonds.

human meibum, i.e., DE-II 70:3 vs. 66:2.

In comparison to the lipid classes discussed above, the pPIS spectra for DE-IIs were more complicated due to the presence of two fatty acid moieties (Figs. 5a & c, Supplementary Figs. S18 & S19). DE-II pPIS spectra were not as straightforward as those of CEs or DE-Is that have only one common product ion (Figs. 4c, 5 b & d) and they were more complicated than those of WEs, which have a set of characteristic product ions depending on only one fatty acid moiety therein (Fig. 4a). In contrast, DE-IIs can produce two sets of product ions for each fatty acid moiety. It is beyond the scope of this study to comprehensively analyze all DE-II molecular species. Instead, only DE-IIs containing FA 18:1, the most abundant fatty acid moiety, were compared. The product ion corresponding to protonated FA18:1 with loss of one water molecule, i.e., *m/z* 265.253, was the highest characteristic product ion (Fig. 5a & c), and the corresponding pPIS spectrum exhibited the highest S/N. However, the S/N was still not high enough to differentiate between some diesters based on the isotopic pattern (Supplementary Fig. S18). Only the 12 most abundant species were confidently identified (Supplementary Table S3). Interestingly, the overall chain length of this set of diesters in tree shrew meibum was again longer than that of human meibum. The most abundant DE-II is FA 18:1/Diol-FA 50:2 (DE-II 68:3) in both species. However, the second most abundant DE-II in tree shrew meibum is FA 18:1/Diol-FA 52:2 (DE-II 70:3), while FA 18:1/Diol-FA 48:2 (DE-II 66:3) is the second most abundant DE-II in human meibum. The observation of longer chain DE-IIs in tree shrew meibum based on MS/MS^{all} is consistent with the corresponding peaks in the MS spectrum.

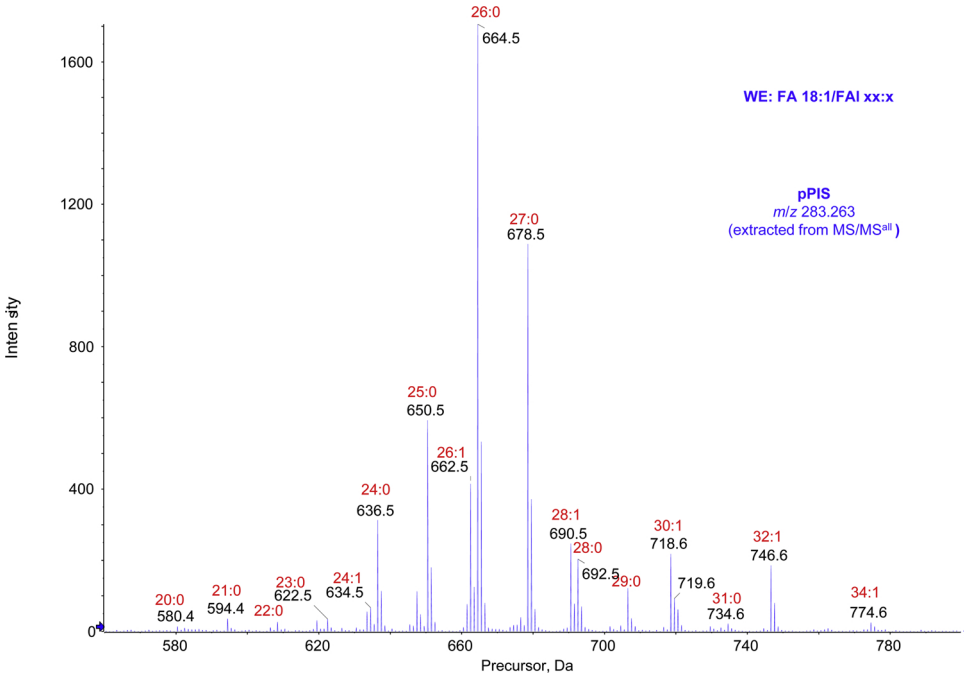

Fig. 8. Pseudo precursor ion scanning spectrum of *m/z* 283.263 ± 0.025, extracted from positive ion mode MS/MS^{all} analysis of tree shrew meibum. The peaks correspond to fatty acid 18:1-based wax esters (WEs), and only the part of the spectrum corresponding to these WEs is shown. Abbreviations for the lipid moieties are as follows: FA, fatty acid; FAl, fatty alcohol. The two numbers labeling each peak, separated by a colon, represent the total number of carbon atoms and the number of double bonds in the FAl moiety of the WE ion.

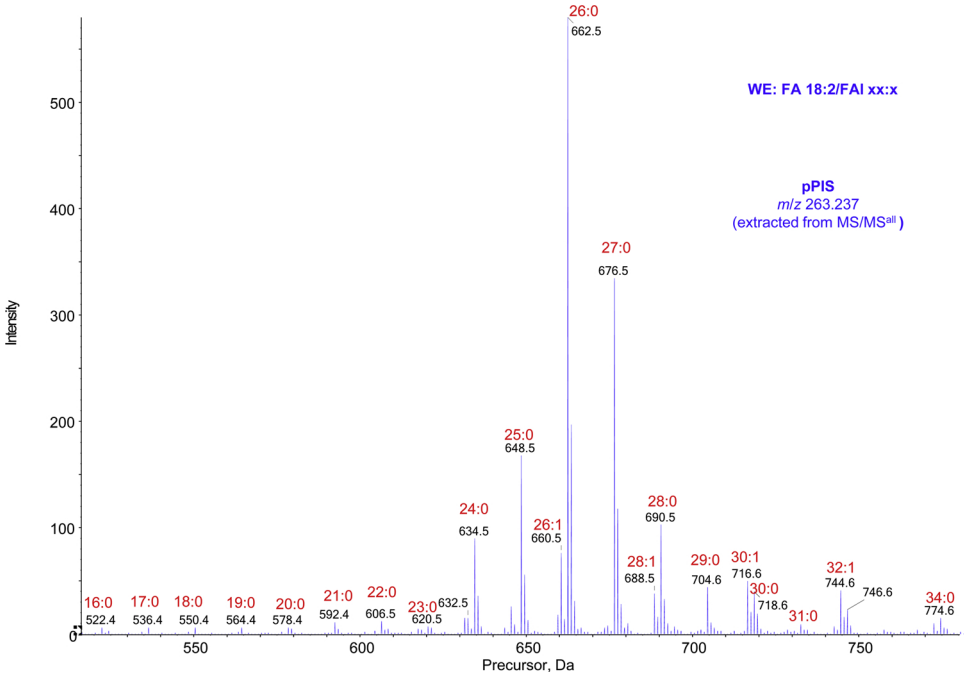

Fig. 9. Pseudo precursor ion scanning spectrum of m/z 263.237 ± 0.025, extracted from positive ion mode MS/MS^{all} analysis. As the product ion m/z 263.237 corresponds to protonated FA 18:2 with loss of a water molecule, the peaks correspond to fatty acid 18:2-based wax esters (WEs). Only the part of the spectrum that corresponds to these WEs is shown. Abbreviations for the lipid moieties are as follows: FA, fatty acid; FAl, fatty alcohol. The two numbers labeling each peak, separated by a colon, represent the total number of carbon atoms and the number of double bonds in the FAl moiety of the WE ion.

3.2.5. Triacylglycerols

In the MS spectrum, a total of 40 TGs were detected (Supplementary Table S1). The compositions of the lipid species of TGs in tree shrew meibum (Fig. 2) appeared similar to those in human meibum (Chen and Nichols, 2018). However, in contrast to the lipids discussed above, the overall chain length of TGs shown in the MS spectrum (Fig. 2) was similar for tree shrew and human meibum (Brown et al., 2013; Chen et al., 2010, 2013; Chen and Nichols, 2018; Lam et al., 2011). In fact, the relative intensity of longer-chain TGs, such as 56:3, was higher in human meibum than in tree shrew meibum (Chen and Nichols, 2018).

The pPIS spectra of TGs, which have three fatty acid moieties, were even more complicated than those of DE-IIs. It is beyond the scope of this study to comprehensively analyze all TG molecular species composed of different acyl chains. Instead, only those containing the most abundant fatty acid moiety, FA 18:1, were compared. The product ion corresponding to protonated FA18:1 with loss of one water molecule was the highest characteristic product ion; however, the abundance of this ion was still much lower than that of the precursor ion or the neutral loss ion (Fig. 4d, Supplementary Fig. S21b).

To increase the S/N, we resorted to pNLS. pNLS was previously found to be ineffective with the default parameters due to the discrepancy between the actual precursor ion and the preset precursor ion (Chen and Nichols, 2018). However, in this study, higher S/N peaks were detected in pNLS when the option “adjust precursor m/z using residual parent” for NLS was selected (Supplementary Fig. S21a). TGs ranging from 46:3 to 55:2 were identified (Supplementary Table S3).

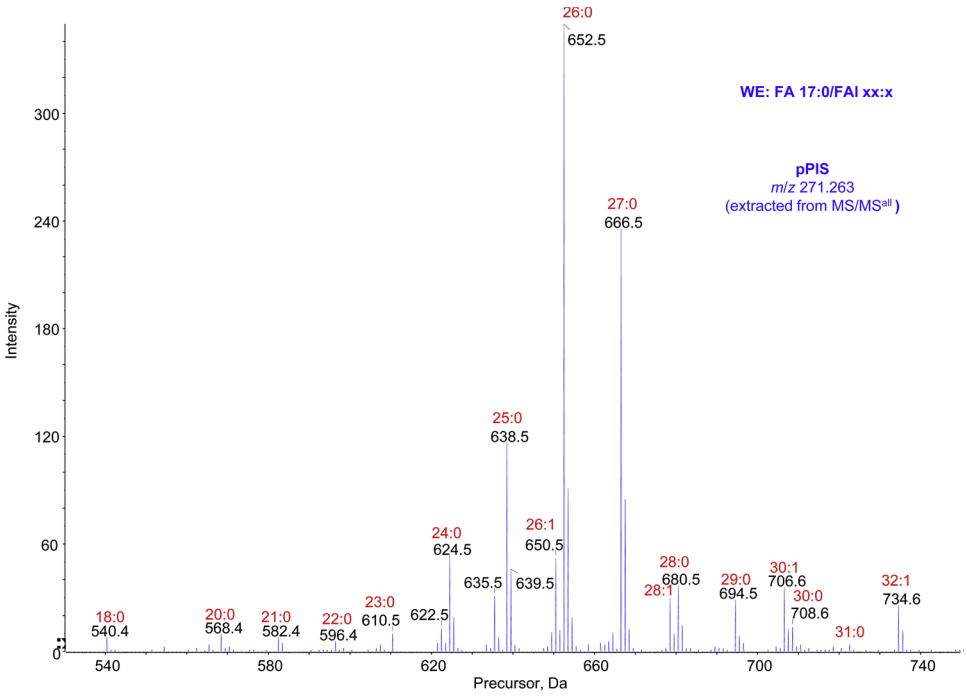

Fig. 10. Pseudo precursor ion scanning spectrum of m/z 271.263 ± 0.025, extracted from positive ion mode MS/MS^{all} analysis. The peaks correspond to fatty acid 17:0-based wax esters (WEs), and only the part of the spectrum that corresponds to these WEs is shown. Abbreviations for the lipid moieties are as follows: FA, fatty acid; FAl, fatty alcohol. The two numbers labeling each peak, separated by a colon, represent the total number of carbon atoms and the number of double bonds in the FAl moiety of the WE ion.

The most abundant FA18:1-based TGs were FA 18:1/2 F A 36:2 and FA 18:1/2 F A 34:1. Consistent with the MS spectra, the overall chain length of this set of TGs in tree shrew meibum was similar to or somewhat lower than that in human meibum (Chen and Nichols, 2018).

3.2.6. (O-acyl)-ω-hydroxy fatty acids

A series of OAHFAs were detected in tree shrew meibum in negative ion mode (Fig. 3). All of the lipid classes discussed above were detected in positive ion mode. A total of 34 OAHFAs were detected in the MS spectrum (Fig. 3, Supplementary Table S2). A striking novel observation in tree shrew meibum is that there appear to be two groups of OAHFAs. The first group contained 24 species with peaks ranging from *m/z* 689 to *m/z* 815, corresponding to OAHFA 45:1 to OAHFA 54:2, while the second group contained 13 species with peaks ranging from *m/z* 781 to *m/z* 928, corresponding to OAHFA 52:2 to OAHFA 62:2. The two groups appeared to share peaks corresponding to OAHFA 52:4 to OAHFA 54:1. Excluding the overlapping peaks, a total of 34 species were detected in MS analysis.

The first group is similar to previous reports of OAHFAs in human meibum. The most abundant OAHFA in tree shrew meibum is the same as in human meibum, OAHFA 50:2 (Brown et al., 2013; Chen et al., 2010; Chen and Nichols, 2018; Lam et al., 2011; Mori et al., 2014). However, the second most abundant OAHFA in tree shrew is longer, OAHFA 52:2 (Fig. 3); in human meibum, OAHFA 48:2 is second most abundant (Brown et al., 2013; Chen et al., 2010; Chen and Nichols, 2018; Lam et al., 2011; Mori et al., 2014).

The second group of putative OAHFAs, to the best of our knowledge, has never been observed in human meibum. The odd-numbered carbon chains of this group also appear to be much less abundant, in contrast to other classes of meibum lipids. This subgroup of OAHFAs centers around 58:2 (Fig. 3).

MS/MS spectra of the two groups of peaks share similar fragmentation patterns, though the chain lengths and saturation levels differ (Figs. 11 & 12). These OAHFAs only generate fatty acid moiety- and hydroxy fatty acid moiety-characteristic product ions, depending on the fatty acid moiety therein. Therefore, for these classes of lipids, a series of pPIS spectra are needed to obtain a complete overview of the lipids. In this report, only two representative pPIS spectra of OAHFAs, FA 18:1 and FA 24:1, were extracted from the MS/MS^{all} acquisition (Fig. 13). A total of 12 and 9 species were identified (Supplementary Fig. S4). MS/MS spectra from the MS/MS^{all} acquisition showed that this second group of lipids were composed of much longer-chain FA moieties, including 24:1, 26:1, and 28:1, while the chain lengths of the hydroxy fatty acid moieties were essentially the same, including 32:1 and 34:1 (Figs. 11–13). Further studies are warranted to confirm the identities of these lipids and determine whether they originated from meibum or surrounding tissues.

The total number of OAHFAs detected by MS/MS^{all} can be calculated from manual analysis (Chen et al., 2010; Chen and Nichols, 2018) of each MS/MS spectrum from the MS/MS^{all} acquisition, which yields a total of 106 species (Supplementary Table S5). In contrast, a total of 196 OAHFAs were found to be present in human meibum (Chen and Nichols, 2018). This higher value is likely due to the higher S/N for human meibum samples.

3.2.7. Free fatty acids

FFAs detected in tree shrew meibum are similar to those previously reported to be present in human meibum (Chen et al., 2010; Chen and Nichols, 2018; Mori et al., 2014). The most abundant FFAs include 24:0, 25:0, 26:0, and 27:0. Unlike the relatively longer chains of other lipid species compared to human meibum, the overall chain length of these FFAs in tree shrew meibum is shorter than that of human meibum. In the tree shrew, the most abundant FFA is 24:0 (Supplementary Table S3); in contrast, FFA 26:0 is the most abundant FFA in human meibum (Chen et al., 2010; Chen and Nichols, 2018; Mori et al., 2014). Furthermore, a series of short-chain FFAs that included 12:0, 14:0, 15:0, and 17:0 was unique to tree shrew meibum. The source(s) of these short-chain FFAs remains unknown.

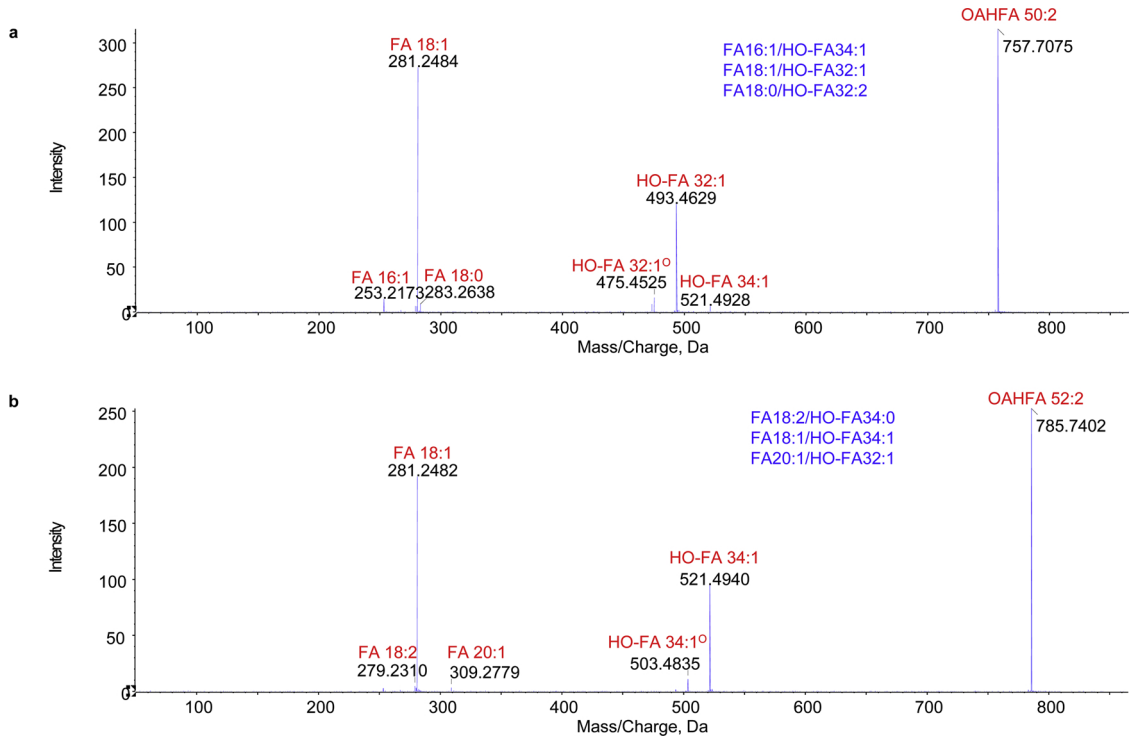

Fig. 11. MS/MS analysis of (*O*-acyl)-ω-hydroxy fatty acids (OAHFAs) in tree shrew meibum similar to those reported in human meibum. a) OAHFA 52:2; b) OAHFA 50:2. The two numbers labeling each OAHFA peak, separated by a colon, represent the total number of carbon atoms and the number of double bonds in the OAHFA ions or the fragment ions. HO-FA, hydroxy fatty acid; FA, fatty acid. The label "^{O}" represents loss of a water molecule.

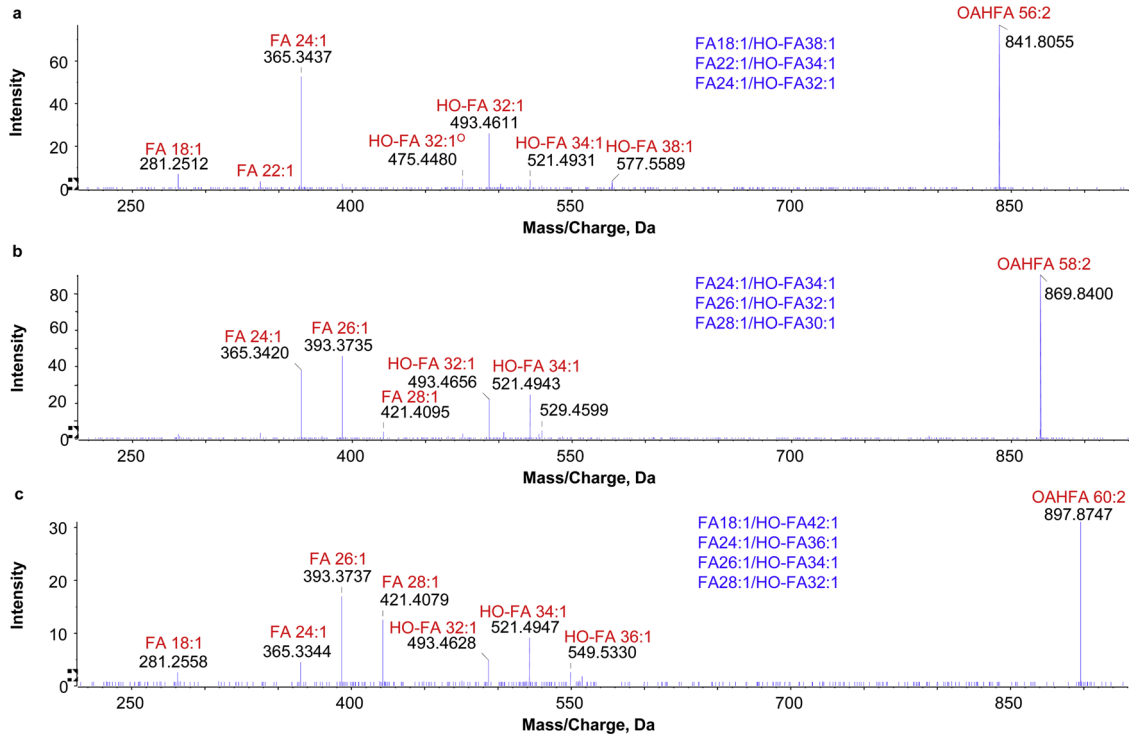

Fig. 12. MS/MS analysis of putative (*O*-acyl)-ω-hydroxy fatty acids (OAHFAs) in tree shrew meibum that were not previously detected in human meibum. a) OAHFA 56:2; b) OAHFA 58:2; and c) OAHFA 60:2. The two numbers labeling each OAHFA peak, separated by a colon, represent the total number of carbon atoms and the number of double bonds in the OAHFA ions or the fragment ions. HO-FA, hydroxy fatty acid; FA, fatty acid. The label "^{O}" represents loss of a water molecule.

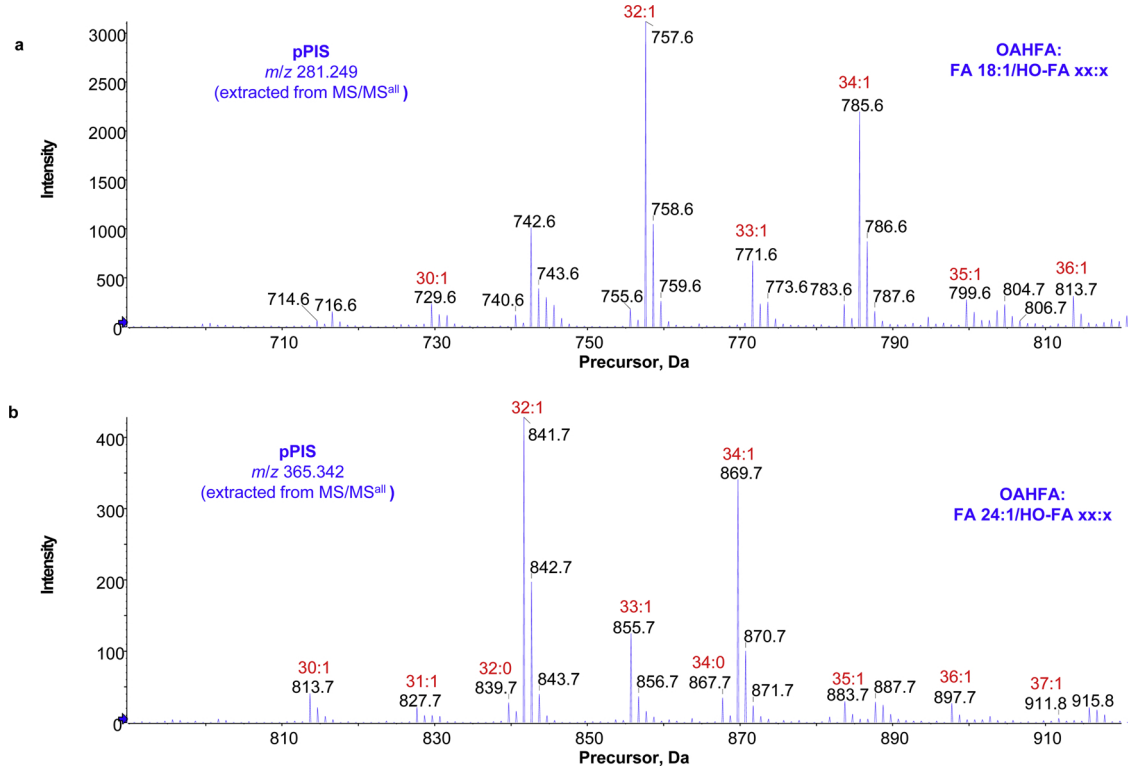

Fig. 13. Pseudo precursor ion scanning spectra extracted from negative ion mode MS/MS^{all} analysis. a) *m/z* 281.249 ± 0.025 and b) *m/z* 365.342 ± 0.025. The peaks correspond to FA 18:1- and FA 24:1-based (*O*-acyl)-ω-hydroxy fatty acids (OAHFAs). The two numbers labeling each OAHFA peak, separated by a colon, represent the total number of carbon atoms and the number of double bonds in the OAHFA ions, excluding the FA 18:1 or FA 24:1 moiety.

3.2.8. Cholesteryl sulfate

Similar to previous reports (Chen et al., 2010; Chen and Nichols, 2018; Lam et al., 2014), cholesteryl sulfate was detected in tree shrew meibum (Fig. 3). The function of cholesteryl sulfate in meibum is not clear, although it has been reported to play an important role in differentiation of epithelial cells in skin (Strott and Higashi, 2003).

Table 2
The numbers of molecular species of each subclass of phospholipids detected in human meibomian gland secretions.[a].

Phospholipids	Number of Molecular Species Detected					
	MS		MS/MS^{all}			
	Pos.	Neg.	Positive		Negative	
Sphingomyelin	19	–	pPIS of 184.074	7	NA	0
Lysophosphatidylcholine	11	–	pPIS of 184.074	11	pNLS of 135.089	4
Phosphatidylcholine	50	–	pPIS of 184.074	20	pNLS of 135.089	14
Lysophosphatidylethanolamine	2	1	pNLS of 141.019	2	pPIS of 140.012	0
Phosphatidylethanolamine	18	8	pNLS of 141.019	16	pPIS of 140.012	6
Lysophosphatidylinositol	–	–	NA	–	pPIS of 241.012	2
Phosphatidylinositol	–	5	NA	–	pPIS of 241.012	16
Phosphatidylserine	2	3	pNLS of 185.009	2	pNLS of 87.032	9
Total	102	17	–	58	–	51

[a] pPIS: pseudo precursor ion scanning; pNLS: pseudo neutral loss scanning. The tolerance was ± 0.025.

Cholesteryl sulfate may, therefore, play a similar role in the differentiation of meibomian gland cells and may be shed during holocrine secretion (Knop et al., 2011).

3.2.9. Phospholipids

The amount of phospholipids, including glycerolphospholipids and sphingophospholipids, in human meibum is typically quite low (Brown et al., 2013; Butovich et al., 2007; Chen et al., 2010; Chen and Nichols, 2018; Lam et al., 2011; Saville et al., 2011). Unexpectedly, in this study we detected relatively high intensity peaks associated with phospholipids, including PCs in positive ion mode and PEs, PIs, and PSs in negative ion modes (Figs. 2–4b, Supplementary Figs. S1, S22-S41, Table 2, Supplementary Tables S1-S4). pPIS and pNLS spectra were obtained based on the characteristic product ions or neutral losses for PC, PS, PE, and PI (Brügger et al., 1997; Busik et al., 2009).

3.2.9.1. Phosphatidylcholines and lysophosphatidylcholines. Highly abundant PCs, detected in positive ion mode in both the MS (Fig. 2, Supplementary Fig. S1) and MS/MS analyses (Fig. 3b, Supplementary Figs. S22 & S23), included PC 34:2, 34:1, 36:2, and 36:1. In the MS spectrum, a total of 50 PCs were identified (Supplementary Table S3). The expression pattern of these PCs was different from PCs detected in human meibum, which included high intensity peaks for odd-numbered carbon chain PCs (Chen and Nichols, 2018; Saville et al., 2011). A total of 11 LPCs were also detected in either the MS spectra or the pPIS spectra (Supplementary Tables S1 & S3, Supplementary Figs. S24 & S25).

Interestingly, a set of peaks detected in negative ion mode MS and MS/MS^{all} appears to correspond to PCs with non-covalent interaction of a molecule of 76.017 Da. These peaks include *m/z* 832.5732, *m/z* 834.5875, *m/z* 860.6025, and *m/z* 862.6170, which represent adducts of PC 34:2, 34:1, 36:2, and 36:1 (Supplementary Table S3, Supplementary Figs. S26-S29). Indeed, the protonated forms of these corresponding PCs were detected with high intensities in positive ion mode (Fig. 2). Similar PC adducts were previously reported in negative ion mode MS/MS analysis of the retina (Busik et al., 2009) and were supported by experiments with PC standards (Zhang and Reid, 2006). By varying the solvents and using isotope-labeled PCs, the 76-Da molecule that forms a complex with PC was determined to be CH_3OCOOH (methylcarbonic acid). This molecule was proposed to be the product of two-step reactions involving hydroxide, carbon dioxide, and methanol (Zhang and Reid, 2006). A total of 10 PCs with the adduct were identified from MS (Supplementary Fig. S30, Supplementary Table S4), corresponding to $CH_3OCOOH + (CH_3)_3N$ (Busik et al., 2009).

3.2.9.2. Sphingomyelins. SMs were detected in positive ion mode in much lower abundance compared to PCs. In the MS spectrum, a total of 19 SMs were identified (Supplementary Table S2, Supplementary Figs. S22 & S31). SM peaks were separated from PC peaks in the MS spectrum. However, it was difficult to differentiate SMs from isotopic peaks of PCs in MS/MS^{all} spectra. Although more SMs may be present, only those matching isotopic patterns were considered. Some of these SMs appeared consistent with those found in human meibum (Chen and Nichols, 2018).

3.2.9.3. Phosphatidylethanolamines and lysophosphatidylethanolamines. PEs were detected in both positive and negative ion modes. In positive ion mode, a total of 18 PEs and 2 LPEs were detected in the MS analysis (Supplementary Tables S1), and a total of 16 PEs and 2 LPEs were detected by pNLS (Supplementary Figs. S32 & S33, Supplementary Table S3). In negative ion mode, a total of 8 PEs and 1 LPE were identified in MS analysis (Fig. 3, Supplementary Tables S4, Supplementary Figs. 34 & 35). Neither PEs nor LPEs were detected in human meibum (Chen and Nichols, 2018).

3.2.9.4. Phosphatidylserines. PSs were also detected in tree shrew meibum in both positive and negative ion modes. In positive ion mode, only 2 PSs were detected in both the MS (Supplementary Table S1) and MS/MS spectra (Supplementary Figs. S36 & S37, Supplementary Table S3). In contrast, detection of PSs was higher in negative ion mode: 3 PSs and 9 PSs were detected in MS (Fig. 3, Supplementary Table S2) and MS/MS (Supplementary Figs. S38 & S39, Supplementary Table S4) spectra, respectively. Peaks corresponding to PSs were difficult to find in the MS spectra due to overlapping peaks. PSs were not detected in human meibum (Chen and Nichols, 2018).

3.2.9.5. Phosphatidylinositols and lysophosphatidylinositols. PIs were only detected in negative ion mode. A total of 5 PIs were detected in the MS analysis (Fig. 3, Supplementary Tables S2), and a total of 2 LPIs and 16 PIs were detected by pPIS (Supplementary Figs. S40 & S41, Supplementary Table S4). Again, levels of all of these phospholipids are negligible in human meibum under the same conditions (Chen and Nichols, 2018). Therefore, it is likely that these lipids originated from either immature meibomian gland cells or from contamination by surrounding tissues.

3.3. Implications from comparison of the lipid profiles of tree shrew meibum and human meibum

A monolayer-thick lipid layer has previously been reported to make up a dense inner layer of the tear film lipids in a rat model, together with a looser outer layer (Chen et al., 1997). It is likely that this monolayer is critical for the function of these lipids in reducing evaporation of tear film. As the most abundant lipid species in meibum and tear film, WEs, CEs, and DEs (Chen et al., 2013; Nicolaides et al., 1981) are probably the major (if not the only) components of this monolayer.

All of these lipids contain polar ester groups that can interact with water molecules to form a monolayer that occupies the same area, independent of chain length (Langmuir, 1917). Indeed, esters, including ethyl esters (Harkins, 1941; Rosano and La Mer, 1956), cholesteryl esters (KWONG et al., 1971; Millar and King-Smith, 2012) and wax esters (Paananen et al., 2014), have been reported to be able form a stable monolayer at the air/water interface.

If the monolayer formed by WE, CE, and DE is critical to the function of the overall lipid layer of the tear film, then the efficiency of evaporation reduction should increase with the chain length of these lipids (La Mer and Healy, 1965). Therefore, increases in chain length of these lipids in tree shrew meibum are consistent with the low blinking frequency of this animal (Stevens and Livermore, 1978), which is indicative of high tear film stability (Inomata et al., 2018) and lower evaporation. Based on the critical monolayer hypothesis, differences in tree shrew and human meibum lipid profiles could identify candidate lipids that may be important for reduction of tear evaporation. With longer chains in tree shrew meibum than in human meibum, OAHFAs are, therefore, likely candidates. As DE-Is are actually esters of OAHFAs, further studies are warranted to determine whether OAHFAs play a direct role in reducing evaporation or instead work as the intermediates for the synthesis of DE-Is.

In contrast to WEs, CEs, DEs and OAHFAs, the overall chain length of TGs and FFAs in tree shrew meibum appeared to be the same, or even decreased, relative to human meibum. Therefore, these TGs and FFAs are not likely to play an important role in reducing tear evaporation and, instead, are more likely just a component of the cell membrane that is shed along with the lipid droplet during the holocrine secretion process (Knop et al., 2011). These lipids may also be contaminants from other tissues, such as conjunctiva, or secretions from the sebaceous glands of Moll and Zeis. In fact, we found that some of the samples we collected were predominantly composed of TGs, particularly 54:3, which is indicative of sebum contamination (Thiboutot, 2004).

Phospholipids, typically negligible in human meibum, were of high abundance in the spectra of tree shrew meibum. The highly abundant phospholipids that were detected, including PC 34:1 and PC 36:2, are common components of epithelial cells (Brügger et al., 1997). These phospholipids likely originated from either immature meibomian gland cells (due to rough, forced meibum expression) or from contamination by eyelid surface cells. Levels of polar lipids in human meibum have been shown to decrease with gentler expression methods (Nicolaides et al., 1981), while more forceful expression of meibum yields higher amounts of phospholipids (Kunnen et al., 2016).

Interestingly, lipids with relatively shorter chain lengths, including FFAs, TGs, and phospholipids, are known to bind to lipocalin (Glasgow et al., 1995), a predominant protein in tears (Dartt, 2011). Therefore, these lipids, which presumably interfere with the effects of the tear film lipid layer, can be sequestered away from the surface of the tear film via lipocalin binding.

It is worth noting that the conventional belief that the lipid layer retards evaporation has been challenged (Georgiev et al., 2017; Sledge et al., 2016). Therefore it is clear that additional studies are needed in order to reach a consensus on the function of the lipid layer in maintaining homeostasis of the ocular surface.

4. Conclusions

Using a newly developed MS/MS^{all} shotgun lipidomics method, we profiled the lipids present in tree shrew meibum. The overall pattern looks quite similar to that of human meibum, suggesting that the tree shrew can serve as a model for dry eye studies. Interestingly, we also identified many interesting differences between tree shrew and human meibum, including much longer chain lengths of DEs and OAHFAs. As not all lipids in meibum are expected to be active due to holocrine secretion, these differences could serve as a means to identify candidate components of the tear film lipid layer important for inhibiting evaporation.

Conflict of interest

The authors declare no conflict of interest.

Acknowledgements

The authors thank Dr. Timothy Gawne for providing the tree shrew eyelids, Dr. Kelly Nichols for encouraging the study of meibum in tree shrew, and Dr. Kelly Nichols, Dr. Timothy Gawne, and Dr. Thomas Norton for helpful discussions. This work was supported by National Institutes of Health GrantsS10 RR027822 and P30 EY003039.

Appendix A. Supplementary data

Supplementary data associated with this article can be found, in the online version, at https://doi.org/10.1016/j.chemphyslip.2019.01.003.

References

Barabino, S., Chen, W., Dana, M.R., 2004. Tear film and ocular surface tests in animal models of dry eye: uses and limitations. Exp. Eye Res. 79, 613–621.
Barabino, S., Dana, M.R., 2004. Animal models of dry eye: a critical assessment of opportunities and limitations. Invest. Ophthalmol. Vis. Sci. 45, 1641–1646.
Borchman, D., Foulks, G.N., Yappert, M.C., Kakar, S., Podoll, N., Rychwalski, P., Schwietz, E., 2012. Physical changes in human meibum with age as measured by infrared spectroscopy. Ophthalmic Res. 44, 34–42.
Borchman, D., Sledge, S., Michiel, H., Dennis, E., Gerlach, D., Bhola, R., 2015. Lipid hydrocarbon chain conformation of surface lipid films by raman spectroscopy and the rate of evaporation. Invest. Ophthalmol. Vis. Sci. 56 1643-1643.
Brown, S.H., Kunnen, C.M., Duchoslav, E., Dolla, N.K., Kelso, M.J., Papas, E.B., Lazon de la Jara, P., Willcox, M.D., Blanksby, S.J., Mitchell, T.W., 2013. A comparison of patient matched meibum and tear lipidomes. Invest. Ophthalmol. Vis. Sci. 54, 7417–7424.
Brügger, B., Erben, G., Sandhoff, R., Wieland, F.T., Lehmann, W.D., 1997. Quantitative analysis of biological membrane lipids at the low picomole level by nano-electrospray ionization tandem mass spectrometry. Proc. Natl. Acad. Sci. U.S.A. 94, 2339–2344.
Busik, J.V., Reid, G.E., Lydic, T.A., 2009. Global analysis of retina lipids by complementary precursor ion and neutral loss Mode tandem mass spectrometry. In: In: Armstrong, D. (Ed.), Lipidomics Volume 1. Methods and Protocols. Humana Press, Totowa, NJ, pp. 33–70.
Butovich, I.A., Uchiyama, E., McCulley, J.P., 2007. Lipids of human meibum: mass-spectrometric analysis and structural elucidation. J. Lipid Res. 48, 2220–2235.
Butovich, I.A., Wojtowicz, J.C., Molai, M., 2009. Human tear film and meibum. Very long chain wax esters and (O-acyl)-omega-hydroxy fatty acids of meibum. J. Lipid Res. 50, 2471–2485.
Butovich, I.A., Borowiak, A.M., Eule, J.C., 2011. Comparative HPLC-MS analysis of canine and human meibomian lipidomes: many similarities, a few differences. Sci. Rep. 1, 24.
Butovich, I.A., Lu, H., McMahon, A., Eule, J.C., 2012. Toward an animal model of the human tear film: biochemical comparison of the mouse, canine, rabbit, and human meibomian lipidomes. Invest. Ophthalmol. Vis. Sci. 53, 6881–6896.
Cao, J., Yang, E.B., Su, J.J., Li, Y., Chow, P., 2003. The tree shrews: adjuncts and alternatives to primates as models for biomedical research. J. Med. Primatol. 32, 123–130.
Carr, S.A., Huddleston, M.J., Bean, M.F., 1993. Selective identification and differentiation of N-and O-linked oligosaccharides in glycoproteins by liquid chromatography-mass spectrometry. Protein Sci. 2, 183–196.
Chen, H.B., Yamabayashi, S., Ou, B., Tanaka, Y., Ohno, S., Tsukahara, S., 1997. Structure and composition of rat precorneal tear film. A study by an in vivo cryofixation. Invest. Ophthalmol. Vis. Sci. 38, 381–387.
Chen, J., Green-Church, K.B., Nichols, K.K., 2010. Shotgun lipidomic analysis of human meibomian gland secretions with electrospray ionization tandem mass spectrometry. Invest. Ophthalmol. Vis. Sci. 51, 6220–6231.
Chen, J., Green, K.B., Nichols, K.K., 2013. Quantitative profiling of major neutral lipid classes in human meibum by direct infusion electrospray ionization mass spectrometry. Invest. Ophthalmol. Vis. Sci. 54, 5730–5753.
Chen, J., Green, K.B., Nichols, K.K., 2015. Characterization of wax esters by electrospray ionization tandem mass spectrometry: double bond effect and unusual product ions. Lipids 50, 821–836.
Chen, J., Green, K.B., Nichols, K.K., 2016. Compositional analysis of wax esters in human meibomian gland secretions by direct infusion electrospray ionization mass spectrometry. Lipids 51, 1269–1287.
Chen, J., Keirsey, J.K., Green, K.B., Nichols, K.K., 2017. Expression profiling of nonpolar lipids in meibum from patients with dry eye: a pilot study. Invest. Ophthalmol. Vis. Sci. 58, 2266–2274.
Chen, J., Nichols, K.K., 2018. Comprehensive shotgun lipidomics of human meibomian gland secretions using MS/MS^{all} with successive switching between acquisition polarity modes. J. Lipid Res. 59, 2223–2236.

Dartt, D.A., 2011. Tear lipocalin: structure and function. Ocul. Surf. 9, 126–138.
Ekroos, K., Chernushevich, I.V., Simons, K., Shevchenko, A., 2002. Quantitative profiling of phospholipids by multiple precursor ion scanning on a hybrid quadrupole time-of-flight mass spectrometer. Anal. Chem. 74, 941–949.
Foulks, G.N., 2007. The correlation between the tear film lipid layer and dry eye disease. Surv. Ophthalmol. 52, 369–374.
Georgiev, G.A., Eftimov, P., Yokoi, N., 2017. Structure-function relationship of tear film lipid layer: a contemporary perspective. Exp. Eye Res. 163, 17–28.
Glasgow, B.J., Abduragimov, A.R., Farahbakhsh, Z.T., Faull, K.F., Hubbell, W.L., 1995. Tear lipocalins bind a broad array of lipid ligands. Curr. Eye Res. 14, 363–372.
Han, X., Gross, R.W., 2005. Shotgun lipidomics: electrospray ionization mass spectrometric analysis and quantitation of cellular lipidomes directly from crude extracts of biological samples. Mass Spectrom. Rev. 24, 367–412.
Han, X., Yang, K., Gross, R.W., 2012. Multi-dimensional mass spectrometry-based shotgun lipidomics and novel strategies for lipidomic analyses. Mass Spectrom. Rev. 31, 134–178.
Harkins, W.D., 1941. A general thermodynamic theory of the spreading of liquids to form duplex films and of liquids or solids to form monolayers. J. Chem. Phys. 9, 552–568.
Huddleston, M.J., Annan, R.S., Bean, M.F., Carr, S.A., 1993. Selective detection of phosphopeptides in complex mixtures by electrospray liquid chromatography/mass spectrometry. J. Am. Soc. Mass Spectrom. 4, 710–717.
Inomata, T., Iwagami, M., Hiratsuka, Y., Fujimoto, K., Okumura, Y., Shiang, T., Murakami, A., 2018. Maximum blink interval is associated with tear film breakup time: a new simple, screening test for dry eye disease. Sci. Rep. 8, 13443.
King-Smith, P.E., Hinel, E.A., Nichols, J.J., 2010. Application of a novel interferometric method to investigate the relation between lipid layer thickness and tear film thinning. Invest. Ophthalmol. Vis. Sci. 51, 2418–2423.
Knop, E., Knop, N., Millar, T., Obata, H., Sullivan, D.A., 2011. The international workshop on meibomian gland dysfunction: report of the subcommittee on anatomy, physiology, and pathophysiology of the meibomian gland. Invest. Ophthalmol. Vis. Sci. 52, 1938–1978.
Kunnen, C.M., Brown, S.H., Lazon de la Jara, P., Holden, B.A., Blanksby, S.J., Mitchell, T.W., Papas, E.B., 2016. Influence of meibomian gland expression methods on human lipid analysis results. Ocul. Surf. 14, 49–55.
Kwong, C.N., Heikkila, R.E., Cornwell, D.G., 1971. Properties of cholesteryl esters in pure and mixed monolayers. J. Lipid Res. 12, 31–35.
La Mer, V.K., Healy, T.W., 1965. Evaporation of Water: its Retardation by Monolayers: spreading a monomolecular film on the surface is a tested and economical means of reducing water loss. Science 148, 36–42.
Lam, S.M., Tong, L., Yong, S.S., Li, B., Chaurasia, S.S., Shui, G., Wenk, M.R., 2011. Meibum lipid composition in Asians with dry eye disease. PLoS One 6, e24339.
Lam, S.M., Tong, L., Duan, X., Petznick, A., Wenk, M.R., Shui, G., 2014. Extensive characterization of human tear fluid collected using different techniques unravels the presence of novel lipid amphiphiles. J. Lipid Res. 55, 289–298.
Langmuir, I., 1917. The constitution and fundamental properties of solids and liquids. II. Liquids. J. Am. Chem. Soc. 39, 1848–1906.
Linton, R.G., Curnow, D.H., Riley, W.J., 1961. The meibomian glands: an investigation into the secretion and some aspects of the Physiology. Br. J. Ophthalmol. 45, 718–723.
Lukoschus, F.S., Mertens, L.J.A.M., Nutting, W.B., Nadchatram, M., 1984. Demodex intermedius sp. Nov. (Acarina: prostigmata: demodicidae) from the meibomian glands of the tree-shrew Tupaia glis (Mammalia: scandentia). Malayan Nature Journal 37, 233–245.
Mathers, W.D., Lane, J.A., 1998. Meibomian gland lipids, evaporation, and tear film stability. Adv. Exp. Med. Biol. 438, 349–360.
Millar, T.J., King-Smith, P.E., 2012. Analysis of comparison of human meibomian lipid films and mixtures with cholesteryl esters in vitro films using high resolution color microscopy. Invest. Ophthalmol. Vis. Sci. 53, 4710–4719.
Montagna, W., Yun, J.S., Silver, A.F., Quevedo Jr, W.C., 1962. The skin of primates. XIII. The skin of the Tree Shrew (Tupaia glis). Am. J. Phys. Anthropol. 20, 431–439.
Mori, N., Fukano, Y., Arita, R., Shirakawa, R., Kawazu, K., Nakamura, M., Amano, S., 2014. Rapid identification of fatty acids and (O-acyl)-omega-hydroxy fatty acids in human meibum by liquid chromatography/high-resolution mass spectrometry. J. Chromatogr. A 1347, 129–136.
Nicolaides, N., Santos, E.C., 1985. The di- and triesters of the lipids of steer and human meibomian glands. Lipids 20, 454–467.
Nicolaides, N., Kaitaranta, J.K., Rawdah, T.N., Macy, J.I., Boswell 3rd, F.M., Smith, R.E., 1981. Meibomian gland studies: comparison of steer and human lipids. Invest. Ophthalmol. Vis. Sci. 20, 522–536.
Norton, T.T., 1999. Animal models of myopia: learning how vision controls the size of the eye. ILAR J. 40, 59–77.
Paananen, R.O., Rantamaki, A.H., Holopainen, J.M., 2014. Antievaporative mechanism of wax esters: implications for the function of tear fluid. Langmuir 30, 5897–5902.
Rosano, H.L., La Mer, V.K., 1956. The rate of evaporation of water through monolayers of esters, acids and alcohols. J. Phys. Chem. 60, 348–353.
Saville, J.T., Zhao, Z., Willcox, M.D., Ariyavidana, M.A., Blanksby, S.J., Mitchell, T.W., 2011. Identification of phospholipids in human meibum by nano-electrospray ionisation tandem mass spectrometry. Exp. Eye Res. 92, 238–240.
Shrestha, R.K., Borchman, D., Foulks, G.N., Yappert, M.C., Milliner, S.E., 2011. Analysis of the composition of lipid in human meibum from normal infants, children, adolescents, adults, and adults with meibomian gland dysfunction using (1)H-NMR spectroscopy. Invest. Ophthalmol. Vis. Sci. 52, 7350–7358.
Simons, B., Kauhanen, D., Sylvanne, T., Tarasov, K., Duchoslav, E., Ekroos, K., 2012. Shotgun lipidomics by sequential precursor ion fragmentation on a hybrid quadrupole time-of-Flight mass spectrometer. Metabolites 2, 195–213.
Sledge, S.M., Khimji, H., Borchman, D., Oliver, A.L., Michael, H., Dennis, E.K., Gerlach, D., Bhola, R., Stephen, E., 2016. Evaporation and hydrocarbon chain conformation of surface lipid films. Ocul. Surf. 14, 447–459.
Sleno, L., 2012. The use of mass defect in modern mass spectrometry. J. Mass Spectrom. 47, 226–236.
Stevens, J.R., Livermore, A., 1978. Eye blinking and rapid eye movement: pulsed photic stimulation of the brain. Exp. Neurol. 60, 541–556.
Strott, C.A., Higashi, Y., 2003. Cholesterol sulfate in human physiology: what's it all about? J. Lipid Res. 44, 1268–1278.
Thiboutot, D., 2004. Regulation of human sebaceous glands. J. Invest. Dermatol. 123, 1–12.
Tomlinson, A., Bron, A.J., Korb, D.R., Amano, S., Paugh, J.R., Pearce, E.I., Yee, R., Yokoi, N., Arita, R., Dogru, M., 2011. The international workshop on meibomian gland dysfunction: report of the diagnosis subcommittee. Invest. Ophthalmol. Vis. Sci. 52, 2006–2049.
Willcox, M.D.P., Argüeso, P., Georgiev, G.A., Holopainen, J.M., Laurie, G.W., Millar, T.J., Papas, E.B., Rolland, J.P., Schmidt, T.A., Stahl, U., Suarez, T., Subbaraman, L.N., Uçakhan, O.Ö., Jones, L., 2017. TFOS DEWS II tear film report. Ocul. Surf. 15, 366–403.
Zhang, X., Reid, G.E., 2006. Multistage tandem mass spectrometry of anionic phosphatidylcholine lipid adducts reveals novel dissociation pathways. Int. J. Mass Spectrom. 252, 242–255.